Separation Science and Technology
Publication details, including instructions for authors and subscription information:
http://www.informaworld.com/smpp/title~content=t713708471

Pure and Binary Adsorption Equilibria of Methane and Carbon Dioxide on Silicalite

Peiyuan Li[a]; F. Handan Tezel[a]
[a] Faculty of Engineering, Department of Chemical Engineering, University of Ottawa, Ottawa, Ontario, Canada

To cite this Article Li, Peiyuan and Tezel, F. Handan(2007) 'Pure and Binary Adsorption Equilibria of Methane and Carbon Dioxide on Silicalite', Separation Science and Technology, 42: 14, 3131 — 3153
To link to this Article: DOI: 10.1080/01496390701512034
URL: http://dx.doi.org/10.1080/01496390701512034

Separation Science and Technology, 42: 3131–3153, 2007

ISSN 0149-6395 print/1520-5754 online
DOI: 10.1080/01496390701512034

Pure and Binary Adsorption Equilibria of Methane and Carbon Dioxide on Silicalite

Peiyuan Li and F. Handan Tezel
Faculty of Engineering, Department of Chemical Engineering, University of Ottawa, Ottawa, Ontario, Canada

Abstract: For the separation of CH_4 and CO_2 from landfill gas, pure and binary adsorption behavior of these gases were studied up to 5 atmosphere pressure at 40, 70, and 100°C for silicalite as the adsorbent. Pure and binary adsorption isotherms were determined experimentally and compared to predicted isotherms by several equilibrium models, as well as the other available data in the literature. Experimental binary isotherms at different concentrations were determined by using three concentration pulse methods (CPM). HT–CPM (Harlick-Tezel CPM) was observed to be the best one to describe the behavior of this binary system. Equilibrium phase diagrams and separation factors were obtained from the experimental binary isotherms. For this system, the integral thermodynamic consistency tests were also shown and discussed.

Keywords: Gas separation, adsorption, carbon dioxide, methane, concentration pulse method, landfill gases, isotherms, silicalite, greenhouse gases

INTRODUCTION

The global environment is a major issue today, and global warming in particular is the focus of much attention. Accumulation of greenhouse gases (GHG) in the atmosphere is responsible for increased global warming of our planet. It is assumed that the increasing concentration of carbon dioxide, mainly from flue gas, automobile, and landfill emissions in the atmosphere is the major contributor to this problem with more than 80% of total GHG emissions (1, 2).

Received 3 December 2006, Accepted 17 April 2007
Address correspondence to F. Handan Tezel, Faculty of Engineering, Department of Chemical Engineering, University of Ottawa, Ottawa, Ontario, Canada. Tel.: 1 (613) 562-5800 ext. 6099; Fax: 1 (613) 562-5172; E-mail: handan.tezel@uottawa.ca

Besides, methane is the most important non-CO_2 GHG responsible for global warming with more than 10% of total GHG emissions. Despite the much smaller amounts of methane released to the atmosphere, the greenhouse warming potential (GWP) of this gas is much higher than carbon dioxide. Therefore, any reduction in methane emissions is important in the short- and medium-term atmosphere reconstruction (1). Landfill gas (LFG) is a multi-component mixture containing mainly methane and carbon dioxide, which constitutes one of the main sources of methane and carbon dioxide emissions, and can be treated as an important resource of directly available methane. This reason, together with a tighter control in emissions to meet Kyoto Protocol targets, puts LFG into consideration for energy production as a source of natural gas, which is mainly methane (1, 3). This requires the removal of CO_2 from landfill gas for the enrichment of methane gas. For this separation, binary gas isotherms of CO_2-CH_4 mixture were obtained by gravimetric, volumetric (4), and concentration pulse chromatographic techniques (5–9) for several adsorbents in the literature. The use of concentration pulse chromatography for adsorbent screening is very attractive since it is relatively inexpensive to setup and easier to operate. A method using the K_p-functions proposed in the literature for determining the binary isotherms from concentration pulse chromatographic data has been given and shown capable of interpreting highly selective binary systems (6, 10–14).

In the work presented in this paper, the adsorption separation of carbon dioxide and methane was studied with silicalite adsorbent. Pure and binary isotherms were obtained by the constant volume and the concentration pulse chromatographic techniques, respectively, and compared to the predicted ones, as well as other experimental data in the literature. Equilibrium phase diagrams, as well as the separation factors were determined from the experimental binary behavior of this system. Also, the thermodynamic consistency tests between pure and binary gas adsorption systems were discussed.

THEORY

Models for mixed-gas adsorption are crucial to the design of adsorptive gas separation processes. They should be capable of predicting the equilibrium amount adsorbed from pure gas isotherms. Because of the lack of experimental mixture data, however, none of the theories or models has been extensively tested. In the literature, there are several gas adsorption isotherm models often used to predict binary systems, including extended Langmuir (15), extended dual-site Langmuir (16), extended Sips (17), ideal adsorbed solution theory (18), Flory-Huggins vacancy solution theory (VST) (19) and the statistical model (20). These models were compared to the experimental mixture isotherms obtained in this study.

For the determination of mixture behavior, concentration pulse chromatographic technique was used. In this technique, a pulse of the sample gas is

injected into the carrier gas stream and passes through the column. The response of the column to the injection is measured as concentration vs. time at the exit of the column. From this response peak a mean retention time of the sample, μ, defined as the first moment of the chromatogram, is determined experimentally (10). Dimensionless Henry's Law constant, K, can be determined from the corrected first moment of the response peak as follows (9, 14, 21, 22):

$$\mu = \frac{\int_0^\infty c(t-\mu_D)dt}{\int_0^\infty cdt} = \frac{L}{v}\left[1 + \frac{(1-\varepsilon)K}{\varepsilon}\right] \tag{1}$$

where t is the time, c is the adsorbate concentration measured at the outlet of the column, L is the column length, ε is the bed porosity, v is the interstitial fluid velocity, K is the dimensionless Henry's Law adsorption equilibrium constant, and μ_D is the dead time.

The dimensionless Henry's Law constants, K, can be converted to a dimensional form, K_p, as follows (22) and gives the slope of the adsorption isotherm for pure component systems.

$$K_p = \frac{K}{RT\rho_P} \tag{2}$$

where T is the absolute temperature, ρ_p is the density of the pellets of the adsorbent and K_p is the dimensional Henry's Law adsorption equilibrium constant.

For the binary mixture systems, the K_p value is related to the slopes of the isotherms of the individual components in the carrier gas mixture. For a binary mixture, the relationship is given as follows (11):

$$K_p = (1-y_1)\frac{dq_1}{dP_1} + y_1\frac{dq_2}{dP_2} \tag{3}$$

where dq_1/dP_1 and dq_2/dP_2 are the slopes of the adsorption isotherms for components 1 and 2, respectively.

This method allows for the experimental evaluation of the binary mixture isotherms when K_p values are determined for different concentrations of the carrier gas (11).

For binary isotherms, both components in the mixed carrier gas are adsorbed and dq_2/dP_2 in the last term of Eq. (3) is not constant. The experimental K_p data represent the combined contribution of both components to the isotherms. The interpretation of the binary K_p data has been treated by several methods in the literature (6, 10, 14, 23). Commonly used methods are listed in Table 1.

The thermodynamics of pure and binary gas adsorption systems has been extensively studied using the Gibbsian surface excess (GSE) model (24), which can be differentiated or integrated using different thermodynamic paths in order to generate various thermodynamic consistency tests. For binary gas adsorption systems, it has been used to develop several

Table 1. Concentration pulse chromatographic methods often used in the literature

MVV-CPM (modified Van der Vlist and Van der Meijden-concentration pulse method) (10, 12, 14)	
4-parameter function	$K_p = A_0 + A_1y_1 + A_2y_1^2 + A_3y_1^3$
Isotherm slope functions	$dq_1/dP_1 = B_0 + B_1y_1 + B_2y_1^2$
	$dq_2/dP_2 = C_0 + C_1y_1 + C_2y_1^2$
Binary isotherm functions	$q_1 = (B_0y_1 + (B_1/2)\ y_1^2 + (B_2/3)\ y_1^3)P$
	$q_2 = [C_0\ (1 - y_1) + C_1/2\ (1 - y_1^2) + C_2/3\ (1 - y_1^3)]P$
MTT-CPM (modified Triebe and Tezel-concentration pulse method) (23)	
5-parameter function	$K_p = A_{-1}\ (\beta + y_1) + A_0 + A_1/(\beta + y_1) + A_2/(\beta + y_1)^2$
Isotherm slope functions	$dq_1/dP_1 = B_0 + B_1/(\beta + y_1) + B_2/(\beta + y_1)^2$
	$dq_2/dP_2 = C_0 + C_1/(\beta + y_1) + C_2/(\beta + y_1)^2$
Binary isotherm functions	$q_1 = [B_0y_1 + B_1 \ln [(\beta + y_1)/\beta] + B_2\, y_1/\beta(\beta + y_1)]P$
	$q_2 = [C_0(1 - y_1) - C_1 \ln [(\beta + y_1)/\beta + 1] + C_2(1 - y_1)/(\beta + 1)(\beta + y_1)]P$
HT-CPM (Harlick and Tezel-concentration pulse method) (6)	
5-parameter function	$K_p = A_1 + A_2y_1 + A_3y_1^2 + A_4 \ln \lvert y_1 + \lambda \rvert$
Isotherm slope functions	$dq_1/dP_1 = B_1 + 2B_2y_1 + B_3/\lvert y_1 + \lambda \rvert$
	$dq_2/dP_2 = C_1 + 2C_2y_1 + C_3/\lvert y_1 + \lambda \rvert$
Binary isotherm functions	$q_1 = [B_1y_1 + B_2y_1^2 + B_3 \ln \lvert (y_1 + \lambda)/\lambda \rvert]P$
	$q_2 = [C_1\ (1 - y_1) + C_2(1 - y_1^2) - C_3 \ln \lvert (y_1 + \lambda)/(1 + \lambda) \rvert]P$

relationships for checking both the thermodynamic consistency between pure and binary gas equilibrium adsorption data as well as the internal thermodynamic consistency of the binary adsorption data itself. These relationships of integral and differential consistency tests have been developed for pure and binary gas adsorption data. The integral test requires the measurement of both pure gas and binary gas adsorption isotherms shown below (25):

$$\left(-\int_0^P \frac{q_2^0}{P}dP\right) - \left(-\int_0^P \frac{q_1^0}{P}dP\right) = \int_0^1 \frac{q_1(1-y_1) - q_2y_1}{y_1(1-y_1)}\,dy_1$$

or

$$\int_0^P \frac{q_1^0}{P}dP - \int_0^P \frac{q_2^0}{P}dP = \int_0^1 \frac{q_1(1-y_1) - q_2y_1}{y_1(1-y_1)}\,dy_1 \tag{4}$$

where q_1^0 and q_2^0 are the amount adsorbed of Components 1 and 2 respectively in the pure gas systems, P is the total pressure, q_1 and q_2 are the amounts

adsorbed of Components 1 and 2, respectively in the binary system, y_1 is the mole fraction of Component 1 in the binary system. The two terms of the left side are the potentials of adsorption at P and T for pure gases 2 and 1, respectively. They can be estimated as a function of P at constant T using the pure gas adsorption isotherm. Thus, the quantity on the left side at any given values of P and T can be evaluated from the pure gas adsorption isotherms of the components of a binary gas mixture. The quantity on the right side at any given values of P and T can be evaluated using the binary gas adsorption isotherm at constant P and T. These two independently measured quantities must be equal; this equality forms the basis for the integral consistency test between pure and binary gas equilibrium adsorption data.

EXPERIMENTAL

Volumetric System

An AccuSorb 2100E Physical Adsorption Analyzer supplied by Micromeritics Instrument Corporation was equipped with high precise pressure transducers and thermocouples. Data acquisition was performed using a National Instruments based data acquisition card and Labview 6.1 on a computer. The adsorbent sample was regenerated at approximately 350°C under vacuum for approximately 20 hours before use. Helium, with a negligible adsorption on the adsorbent, was used to measure the dead volume in the gas phase.

Concentration Pulse Chromatography

A schematic diagram of the experimental apparatus is shown in Fig. 1. The flow rates and compositions of the carrier gases (A) were controlled by two MKS mass flow controllers (B), and set to a total flowrate of 15 cc/min. A mixing chamber (C) was installed after the mass flow controllers to ensure a homogeneous mixture in the carrier gas. The carrier gas passed through the reference side of the thermal conductivity detector (TCD) (E) in the system. It then went through the sample injection valve (F), which introduced a 1 cc pulse of adsorbate sample gas (D) at atmospheric pressure into the mixed carrier gas stream. Then, the carrier and the sample passed through the packed column (G) and the sample side of TCD (E), where the response of the column to the sample injection as a voltage was monitored as a function of time. Data acquisition was performed using a National Instruments based data acquisition card and Labview 6.1 on a computer. The adsorbent was regenerated at 101.3 kPa and 350°C under helium purge for approximately 20 hours before use. The column was packed with zeolite silicalite adsorbent within a Varian 3300 gas chromatograph.

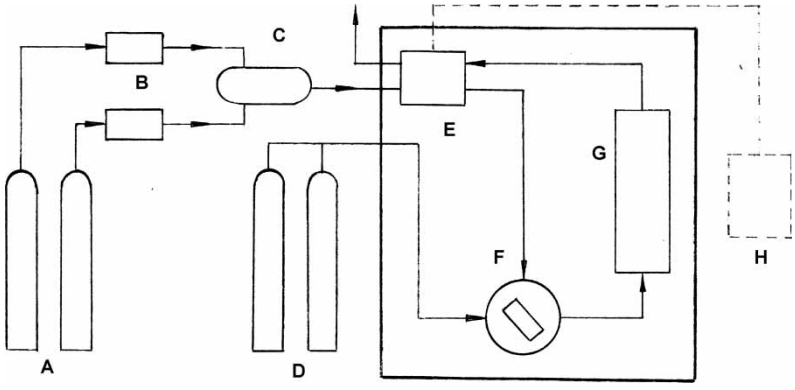

Figure 1. Schematic diagram of the experimental apparatus: A – Carrier gases; B – MKS mass flow controllers; C – Mixing chamber; D – Sample gases; E – TCD; F – Gas injection valve; G – Packed adsorption column within GC oven; H – Computer data acquisition system.

It is noted that there are two methods to determine the pure isotherms for the end-points of the binary isotherms. The first one is volumetric method, which is traditional, popular and reliable which was used in this work. The latter is concentration pulse chromatographic method, in which helium is mixed with the adsorbate and used as the carrier gas. The two methods are consistent with each other according to our study.

When determining binary isotherms, mixed carriers were used without the He gas. For the CO_2-CH_4 system, CH_4 was used as the primary gas. Samples of each gas were injected into the column at different carrier gas concentrations.

It is important to note that the experimental data represents the binary isotherm's effective slope at a particular mixture composition. As the injection volume approaches zero, the K_p values found by both injections should be identical. When CO_2 is injected, the mixture composition increases slightly in CO_2 concentration. When CH_4 is injected, the mixture composition decreases slightly in CO_2 concentration. Therefore, in this study, both adsorbates were injected into the mixed carrier gas and the arithmetic average of the retention times was determined. These average retention times found for CO_2 and CH_4 did not vary by more than 5% for this binary study.

Materials

The adsorbent and sample gases used in the experiments are listed in Tables 2 and 3 respectively. It should be noted that the values of capacities obtained from experiments were corrected with respect to the binder amount in the pellets, assuming that the binder does not adsorb at all.

Table 2. Details of the adsorbent studied

Type	Silicalite
Commercial name	MOLSIV adsorbents
Commercial number	HISIV 3000
Particle form received	1/16 inch extrudate as received
Size used in the column (diameter)	Crushed to 20 × 60 mesh
Content of binder	20 wt%
Particle density	1.131 $g \cdot cm^{-3}$
Void fraction	0.39
Supplier	Universal Oil Products, Des Plaines, IL, USA

Numerical Methods

A non-linear regression was performed in order to determine the parameters for the pure component isotherm fits to the Toth isotherm as well as the K_p regressions. In order to solve the equations given by HT-CPM, MTT-CPM and MVV-CPM, a non-linear equation solver was used. This method was based on Newton's method. In order to determine the optimal values of the B_j and C_j parameters for the HT-CPM, MTT-CPM and MVV-CPM, a non-linear constrained optimization technique was used by using the Solver in MS Excel.

RESULTS AND DISCUSSION

Pure Gas Adsorption of CO_2 and CH_4 by Silicalite

Adsorption equilibrium isotherm data for CO_2 and CH_4 on silicalite pellets were obtained at three different temperatures for pressures up to 5 atm and are given in Fig. 2 as data points. All the adsorption capacity values obtained from experiments were corrected with respect to the binder in this work. The curves going through the data points represent Toth isotherm models at the corresponding temperature. The numbered curves are data

Table 3. Details of the gases used

Gases	Grade	Purity (%)	Supplier
CO_2	Bone dry 3.0	99.9	Praxair Inc., Ottawa
CH_4	Ultra high purity 3.7	99.97	Praxair Inc., Ottawa
He	Ultra high purity 5.0	99.999	Praxair Inc., Ottawa

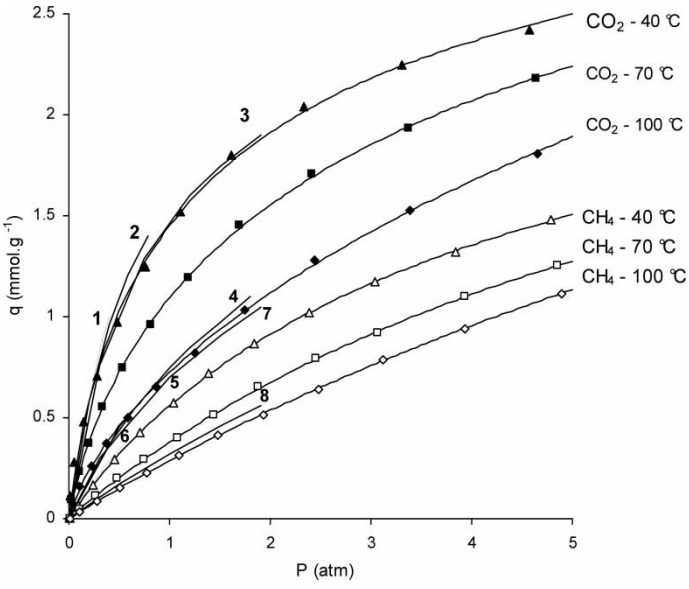

Figure 2. Isotherms for CO_2 and CH_4 on silicalite: The points are experimental data and the curves through the data points are toth isotherm model fits. The numbered curves indicate comparisons with the literature: 1: CO_2-25°C (26); 2: CO_2-31°C (27); 3: CO_2-32°C (28); 4: CO_2-80°C (28); 5: CH_4-23°C (27); 6: CH_4-25°C (26); 7: CH_4-31°C (28); 8: CH_4-81°C (28).

from the literature (as indicated in the figure), given for comparison with the present study. Although the temperatures are not exactly the same, the qualitative comparison with the literature is excellent, with adsorption capacity increasing with decreasing temperature and/or increasing pressure, for both of the adsorbates, since physical adsorption is always exothermic. CO_2 is adsorbed more than CH_4 since the quadrupole moment of carbon dioxide is much higher than that of methane. At low pressure, the slopes of the isotherms of carbon dioxide are very high, and then the slopes decrease rather fast with increasing pressure as the adsorbent sample approach to saturation. However, the slopes of the isotherms of methane hardly decease as pressure increases, isotherms being more linear at high temperature.

By using non-linear regressions, the parameters of different isotherm models were obtained and corresponding parameters are shown in Table 4. For gauging the quality of the non-linear regressions obtained from the different models used, the RMS (root mean square) deviations ($[\Sigma(q_{data}-q_{curve})^2/\mathrm{n}]^{0.5}$) are used and shown in Table 4. When two-parameter models, Langmuir and Freundlich, are compared, Langmuir is better than Freundlich. When three-parameter models were considered, it was observed that all of them, Sips, Flory-Huggins vacancy solution theory (VST), Toth and

Table 4. Parameters and RMS deviations of adsorption models by non-linear regressions

Models		Parameters	CO_2			CH_4		
			40°C	70°C	100°C	40°C	70°C	100°C
Langmuir (2 param.)	$q = q_m BP/1 + BP$	B (atm^{-1})	1.089	0.649	0.332	0.277	0.138	0.071
		q_m (mmol · g^{-1})	2.858	2.834	2.911	2.578	3.128	4.345
		RMS	0.050	0.040	0.038	0.005	0.005	0.003
Freundlich (2 param.)	$q = kP^{1/n}$	k (mmol · g^{-1} · $atm^{-1/n}$)	1.340	1.035	0.713	0.555	0.384	0.292
		n (dimensionless)	2.295	1.938	1.616	1.540	1.306	1.172
		RMS (mmol · g^{-1})	0.106	0.067	0.022	0.037	0.021	0.010
Sips (Langmuir-Freundlich) (3 param.)	$q = q_m(BP)^{1/n}/1 + (BP)^{1/n}$	B (atm^{-1})	0.675	0.337	0.065	0.242	0.137	0.060
		q_m (mmol · g^{-1})	3.431	3.697	6.240	2.752	3.134	4.827
		n (dimensionless)	1.256	1.249	1.349	1.039	1.001	1.019
		RMS (mmol · g^{-1})	0.021	0.012	0.009	0.003	0.005	0.003
Toth (3 param.)	$q = q_m\, BP/[1 + (BP)^n]^{1/n}$	B (atm^{-1})	1.397	0.678	0.100	0.257	0.136	0.053
		q_m (mmol · g^{-1})	3.903	4.885	38.98	2.981	3.166	6.020
		n (dimensionless)	0.604	0.537	0.260	0.864	0.991	0.845
		RMS (mmol · g^{-1})	0.028	0.013	0.011	0.003	0.005	0.003
Flory-Huggins VST (3 param.)	$P = [1/B \cdot q/(1 - q/q_m)]$ exp $[\alpha^2 \cdot q/q_m/(1 + \alpha^2 \cdot q/q_m)]$	B (mmol · g^{-1} · atm^{-1})	3.874	2.608	1.280	0.771	0.434	0.310
		q_m (mmol · g^{-1})	3.082	3.498	5.969	2.976	3.308	5.609
		α_{1v} (dimensionless)	1.020	1.525	2.123	0.806	0.360	0.697
		RMS (mmol · g^{-1})	0.032	0.014	0.019	0.003	0.005	0.003

(*continued*)

Table 4. Continued

Models		Parameters	CO_2 40°C	CO_2 70°C	CO_2 100°C	CH_4 40°C	CH_4 70°C	CH_4 100°C
Multisite Langmuir (3 param.)	$BP = q/q_m/(1 - q/q_m)^n$	B (atm^{-1})	1.002	0.341	0.014	0.180	0.118	0.028
		q_m ($mmol \cdot g^{-1}$)	3.322	6.567	78.01	4.208	3.683	10.97
		n (dimensionless)	1.412	3.881	43.90	2.080	1.248	2.849
		RMS ($mmol \cdot g^{-1}$)	0.049	0.019	0.027	0.003	0.005	0.003
Dualsite Langmuir (4 param.)	$q = q_{m1}B_1P/(1 + B_1\ P) + q_{m2}B_2P/(1 + B_2P)$	B_1 (atm^{-1})	0.782	0.393	0.190	0.004	0.002	0.062
		q_{m1} ($mmol \cdot g^{-1}$)	2.822	2.904	3.492	14.05	5.091	4.729
		B_2 (atm^{-1})	36.44	7.003	11.00	0.347	0.144	0.943
		q_{m2} ($mmol \cdot g^{-1}$)	0.217	0.305	0.173	1.989	2.919	0.029
		RMS ($mmol \cdot g^{-1}$)	0.012	0.019	0.027	0.003	0.005	0.003
Temperature independent Sips	$q = q_m(BP)^{1/n}/[1 + (BP)^{1/n}]$	B (atm^{-1})	0.594	0.343	0.212	0.187	0.143	0.115
		q_m ($mmol \cdot g^{-1}$)	3.614	3.614	3.614	3.108	3.108	3.108
		n (dimensionless)	1.321	1.223	1.149	1.093	1.002	0.936
		RMS ($mmol \cdot g^{-1}$)	0.026	0.026	0.026	0.010	0.016	0.011
Temperature independent Toth	$q = q_mBP/[1 + (BP)^n]^{1/n}$	B (atm^{-1})	1.617	0.640	0.285	0.262	0.172	0.121
		q_m ($mmol \cdot g^{-1}$)	4.649	4.649	4.649	2.533	2.533	2.533
		n (dimensionless)	0.496	0.570	0.635	1.067	1.160	1.283
		RMS ($mmol \cdot g^{-1}$)	0.031	0.015	0.024	0.012	0.018	0.016

Multisite-Langmuir, are better than the two-parameter models because of their increased flexibility. The four-parameter model, Dualsite-Langmuir Model, is better than all the other models used because of its maximum flexibility among the models applied.

For useful description of adsorption equilibrium data at various temperatures, the temperature independent forms of the Toth and Sips equations were also used. By using the data at the three experimental temperatures simultaneously for curve fitting of both temperature independent Sips and Toth equations, optimal parameters shown in Table 5 were obtained. The parameters and RMS deviations at the three temperatures are listed in Table 4. From the parameters given in Table 5 for temperature independent Toth and Sips isotherms, the experimental data are extended to other temperature and pressures.

By using the Clausius-Clapeyron equation, the isosteric heat of adsorption on silicalite was obtained at the limit of zero coverage at 313–373 K with the volumetric method for pure gases: Q_{CO2} is 28.31 kJ · mol^{-1} (compared with 27.2 kJ · mol^{-1} from Dunne et al. (27) and 29.0 kJ · mol^{-1} from Dubinin et al (29)) and Q_{CH4} is 12.52 kJ · mol^{-1} (compared with 12–20 kJ · mol^{-1} from Otto et al. (30)).

The primary requirement for an economic separation process is an adsorbent with sufficiently high selectivity, capacity, and life. The selectivity may depend on a difference in either adsorption kinetics or adsorption equilibrium. Most of the adsorption processes in current use depend on equilibrium selectivity. In considering such processes it is convenient to define an ideal adsorption separation factor:

$$\alpha_{A/B} = \frac{x_A/x_B}{y_A/y_B} \tag{5}$$

Table 5. Optimal parameters determined for the temperature independent Toth and Sips equations for a reference temperature $T_0 = 40^\circ$C

Adsorbates	Parameters	Units	Temperature dependent Toth	Temperature independent Sips
CO_2	χ	Dimensionless	0	0
	q_{m0}	mmol · g^{-1}	4.649	3.614
	B_0	atm^{-1}	1.660	0.603
	Q/RT_0	Dimensionless	10.87	6.439
	n_0	Dimensionless	0.494	1.324
	α	Dimensionless	0.869	0.708
CH_4	χ	Dimensionless	0	0
	q_{m0}	mmol · g^{-1}	2.533	3.108
	B_0	atm^{-1}	0.262	0.187
	Q/RT_0	Dimensionless	4.809	3.068
	n_0	Dimensionless	1.067	1.093
	α	Dimensionless	1.065	0.954

where x_A, x_B, y_A, and y_B are, respectively, the mole fractions of components A and B in adsorbed and fluid phases at equilibrium. If the isotherms are linear or the pressure is small enough for the isotherms to be in the linear range, ideally, the separation factor is given simply by the ratio of the amounts adsorbed for the pure components:

$$\alpha_{i,A/B} = \frac{q_A}{q_B} \tag{6}$$

where q_A and q_B are the amounts adsorbed of components A and B. These equilibrium separation factors are shown as a function of pressure and temperature in Fig. 3. According to the results, both pressure and temperature are very important for the separation. In general, separation factors increase with decreasing pressure and/or temperature. It is difficult to separate the system at high temperature and/or high pressure. For landfill gas, generally, the separation is easier than other applications as the temperature is between 40 and 50°C.

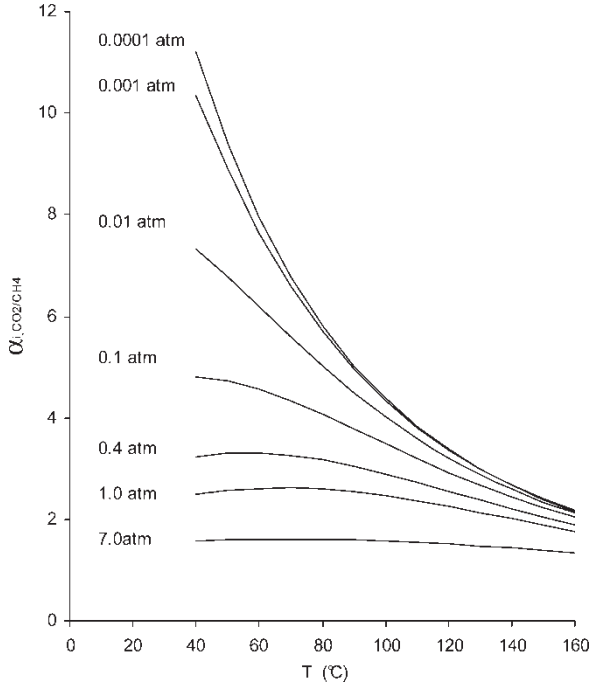

Figure 3. Ideal separation factors for CO_2/CH_4 on silicalite.

Binary Isotherms

After regenerating the silicalite adsorbent, K_p values were determined by increasing the CO_2 mole fraction in CO_2-CH_4 carrier gas from 0% up to 100%. The samples were injected after attaining equilibrium for each concentration change of the carrier gas by noting that the baseline of the response would be steady. The K_p values, as well as their corresponding curve fits for HT-CPM, MTT-CPM and MVV-CPM, as a function of the gas composition are given in Fig. 4. It should be noted that the increment of y_{CO2} is not used in the calculations since the equations of isotherm slope functions in Table 1 are substituted into Eq. (3) to do the calculations. When y_{CO2} is very small at the beginning, K_p decreases extremely fast, so the taken increment of y_{CO2} is very small for obtaining more accurate results in this range. As can be seen from this figure, the best fit was obtained with the HT-CPM. As was proven

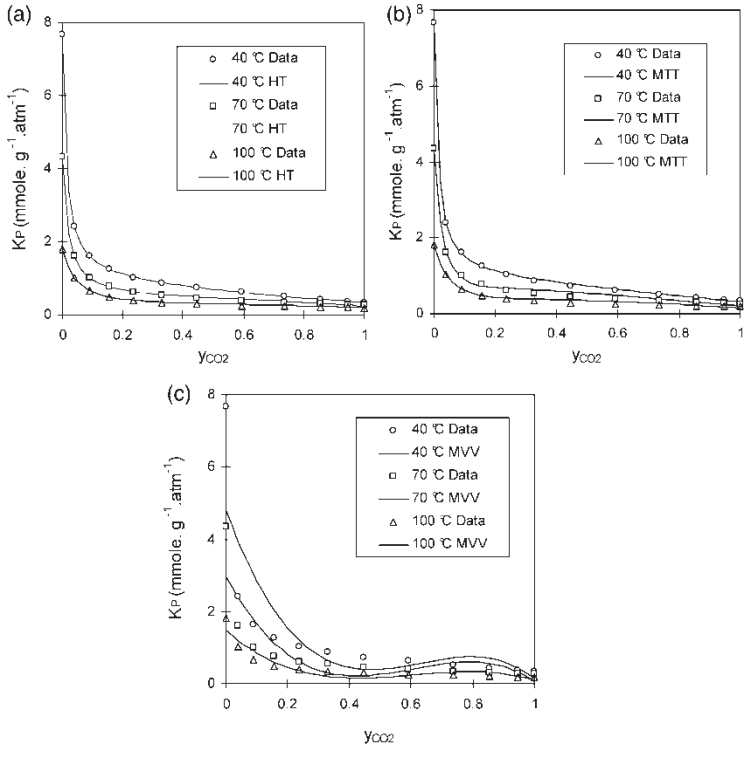

Figure 4. (a) Regressions for CO_2/CH_4 binary K_p with silicalite by HT-CPM at different carrier gas compositions at 1 atm total pressure; (b) regressions for CO_2/CH_4 binary K_p with silicalite by MTT-CPM at different carrier gas compositions at 1 atm total pressure; (c) regressions for CO_2/CH_4 binary K_p with silicalite by MVV-CPM at different carrier gas compositions at 1 atm total pressure.

before, this method is a more versatile method, which would accommodate more non-ideal systems, where the adsorption capacities of the two adsorbates are very different from each other (5).

To quantify the non-linear regressions for these three concentration pulse methods, the RMS (root mean square) deviations ($[\Sigma(K_{p,data} - K_{p,curve})^2/n]^{0.5}$) were used and shown in Table 6. It was observed that the best fit was given by the HT-CPM. Therefore, the HT-CPM was used to describe these systems for our further study of this binary system.

The experimental binary isotherms for CO_2-CH_4 with silicalite were obtained at three temperatures and are given in Fig. 5 in comparison with the predicted ones. When y_{CO2} increases, the CO_2 adsorption capacity, q_{CO2}, increases and the CH_4 adsorption capacity, q_{CH4}, decreases as expected. The total adsorbed capacity, q_{total}, has a minimum when y_{CO2} is smaller than 0.2, due to a sharp decrease in CH_4 adsorption capacity because of the competitive adsorption by CO_2. The gas composition of CO_2 at which this minimum occurs, increases with temperature. For landfill gas, whose y_{CO2} is around 0.45, the CO_2 adsorption capacity is much higher than that of CH_4; therefore, this trend in adsorption capacities for these gases is very promising for silicalite as an adsorbent for applications in CO_2 removal from landfill gas.

To predict the adsorption behavior of the binary system from pure gas systems, six models were tried: extended Langmuir, extended Dualsite Langmuir, extended Sips, ideal adsorbed solution theory, Flory-Huggins VST (Vacancy Solution Theory), and the Statistical Model. For estimating and comparing the quality of the six binary model predictions, the RMS deviations from the binary experimental data ($[\Sigma(q_{data} - q_{curve})^2/n]^{0.5}$) were used and are listed in Table 7. When predicted and experimental isotherms are compared, it was observed that all the six prediction models are similar and there is a rather big difference between the predicted and the experimental isotherms. In Fig. 5, experimental binary isotherms are compared with their counterparts predicted by the Flory-Huggins VST isotherms. Since all the models used for the prediction of the binary system gave very similar results, only the Flory-Huggins VST data are shown in Fig. 5. As can be

Table 6. RMS deviations ($[\Sigma(K_{p,data} - K_{p,curve})^2/n]^{0.5}$) in $mmole \cdot g^{-1} \cdot atm^{-1}$ of concentration pulse chromatographic methods for CO_2-CH_4 binary system on silicalite

CPM	40°C	70°C	100°C
HT	0.009	0.019	0.020
MTT	0.027	0.063	0.038
MVV	1.061	0.536	0.152

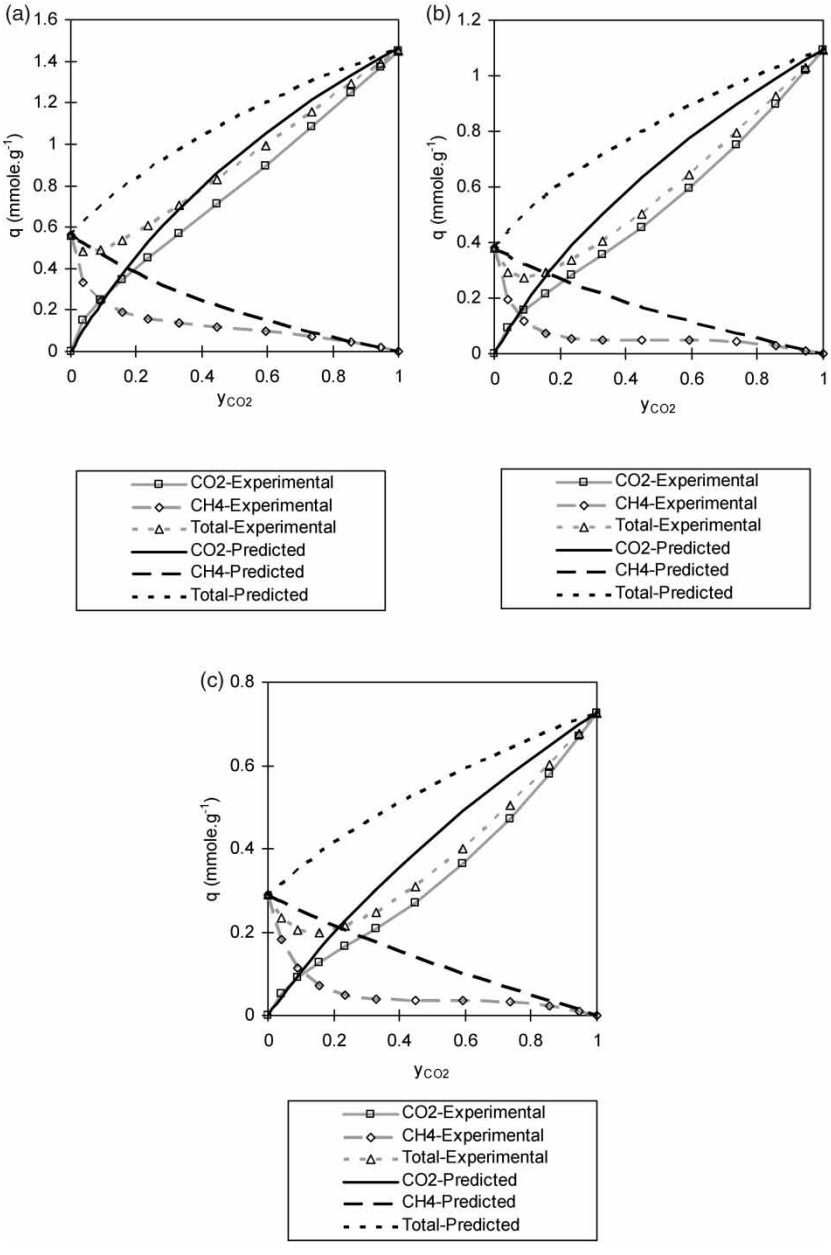

Figure 5. (a) CO_2/CH_4 binary isotherms with silicalite at 40°C and at 1 atm. total pressure experimental by HT-CPM and predicted by Flory-Huggins VST; (b) CO_2/CH_4 binary Isotherms with silicalite at 70°C and at 1atm. total pressure experimental by HT-CPM and predicted by Flory-Huggins VST; (c) CO_2/CH_4 binary isotherms with silicalite at 100°C and at 1 atm total pressure experimental by HT-CPM and predicted by Flory-Huggins VST.

Table 7. RMS deviations ($[\Sigma(q_{data} - q_{curve})^2/n]^{0.5}$) in mmole $\cdot$ g^{-1} of predicted isotherms from the experimental ones for CO_2-CH_4 binary system on silicalite

Models	Capacity	40°C	70°C	100°C
Extended	q_{CO2}	0.096	0.099	0.062
Langmuir	q_{CH4}	0.158	0.147	0.107
	q_{total}	0.205	0.210	0.148
Extended Dualsite	q_{CO2}	0.150	0.135	0.082
Langmuir	q_{CH4}	0.060	0.062	0.108
	q_{total}	0.093	0.167	0.178
Extended Sips	q_{CO2}	0.098	0.113	0.090
	q_{CH4}	0.163	0.150	0.113
	q_{total}	0.242	0.243	0.193
Ideal adsorbed	q_{CO2}	0.099	0.098	0.060
solution theory	q_{CH4}	0.155	0.148	0.109
	q_{total}	0.205	0.210	0.149
Flory-Huggins	q_{CO2}	0.097	0.115	0.078
VST	q_{CH4}	0.146	0.141	0.105
	q_{total}	0.203	0.231	0.166
Statistical method	q_{CO2}	0.098	0.097	0.059
	q_{CH4}	0.149	0.145	0.108
	q_{total}	0.193	0.204	0.146

seen from these comparisons, the predicted isotherms over predict the real ones at all temperatures studied.

The phase diagrams at different temperatures were determined from the experimental binary isotherms and are shown in Fig. 6, together with comparison with the predictions from the Flory-Huggins VST isotherms. Within the temperature range studied, 70°C data gave the best separation, since it was the furthest from the 45° line. Realistic experimental data gave better separation than the Flory-Huggins VST predicted under comparable conditions. Additionally, all other five models looked very similar to the Flory-Huggins VST data shown in Fig. 6 and have considerable differences with the real binary system behavior obtained. This lack of success for model predictions was also observed for CO_2-CH_4 with ZSM-5-280 by Harlick and Tezel (8). Therefore, they can only be used for rough estimation for the binary behavior when there are no binary experimental data available.

Compared with the literature, at 40°C the $x-y$ diagram obtained in this study is similar to the ones given by Harlick and Tezel in 2001 (6) for ZSM-5 under the same conditions, since silicalite and ZSM-5 have the same structure.

According to Equation (6), the equilibrium separation factors at three temperatures can be calculated for different values of y_{CO2} and are shown in Fig. 7. The actual equilibrium separation factors are higher than 5, so the binary system can be separated on silicalite. These separation factors

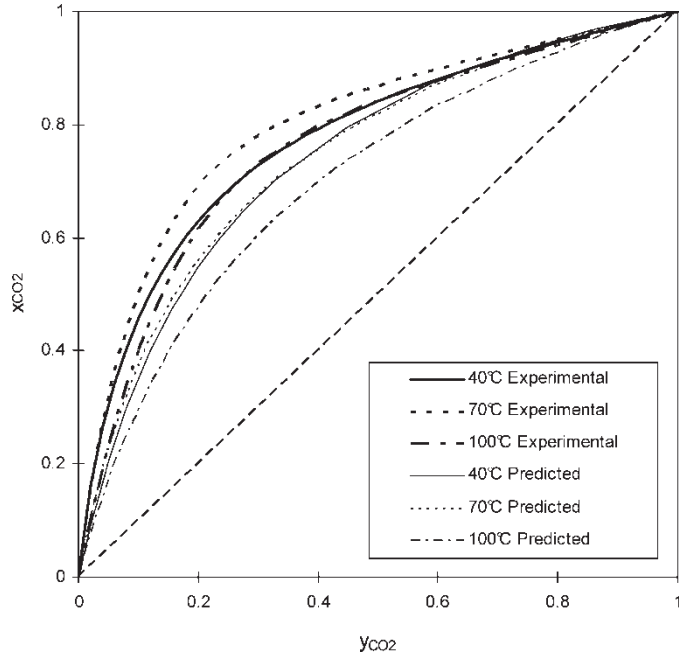

Figure 6. $x-y$ diagram for CO_2/CH_4 binary system with silicalite at 1 atm total pressure experimental by HT-CPM and predicted by Flory-Huggins VST. Harlick and Tezel's data (6) for ZSM-5-30 and ZSM-5-280 gave very similar results to 40°C in this study.

calculated from actual binary behavior are much better than the ones predicted from the pure isotherms. When the compositions are near pure systems (0 or 1), predicted separation factors are near actual ones. At that time, we can use predicted separation factors to do rough estimations if we do not have experimental binary data. The actual selectivity is good and temperature influence the separation factor apparently when y_{CO2} is below 0.6. The actual selectivity decreases with increasing y_{CO2} when CO_2 concentration in the landfill gas is over 30%. Therefore, the actual selectivity is better for low CO_2 concentration landfill gas in the real applications. Temperature hardly influences the separation factor when y_{CO2} is over 0.6. For the practical separation of landfill gases, the system can be separated as the equilibrium separation factors are over 6 when y_{CO2} is around 0.45 for a typical landfill gas.

According to Equation (4), the integral thermodynamic consistency test between pure and binary equilibrium adsorption data is shown in Table 8. For the binary systems, the integrands of the right side as functions of y_1 (y_{CO2}) can be plotted and the areas under these curves between y_1 (y_{CO2}) = 0 and y_1 (y_{CO2}) = 1 are listed. For pure systems, the integrands of the left side as functions of P can be plotted and the areas under these

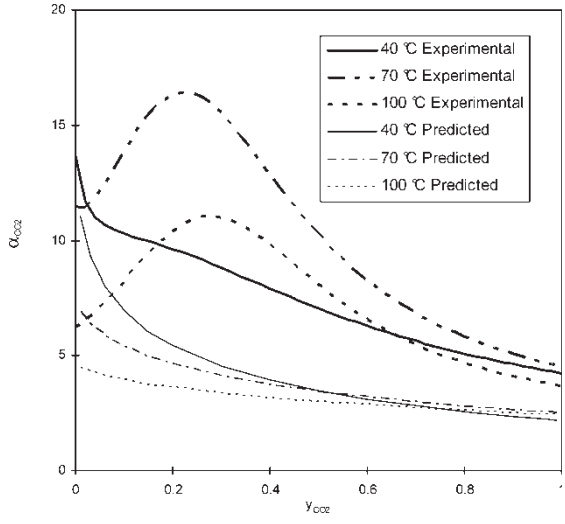

Figure 7. Equilibrium separation factor curves for CO_2/CH_4 binary systems: experimental from binary isotherms and predicted from pure isotherms.

curves between $P = 0$ and $P = 1$ atm are listed. It should be pointed out that the ranges of pressure of the pure systems are the same as the ranges of the partial pressures of the two components as the total pressure of binary system is 1 atm

Table 8. The integral thermodynamic consistency test between pure and binary carbon dioxide (1) – methane (2) equilibrium adsorption data on silicalite using Eq. (4)

Temperature	°C	40	70	100
RHS: $\int_0^1 \frac{q_1(1-y_1)-q_2y_1}{y_1(1-y_1)}dy_1$	$\text{mmol} \cdot \text{g}^{-1}$	1.6183	1.0916	0.6168
1st term in LHS: $\int_0^1 \frac{q_1^0}{P}dP$	$\text{mmol} \cdot \text{g}^{-1}$	2.3084	1.5809	1.0193
2nd term in LHS: $\int_0^1 \frac{q_2^0}{P}dP$	$\text{mmol} \cdot \text{g}^{-1}$	0.6456	0.4036	0.3138
LHS: $\int_0^1 \frac{q_1^0}{P}dP - \int_0^1 \frac{q_2^0}{P}dP$	$\text{mmol} \cdot \text{g}^{-1}$	1.6628	1.1771	0.7055
$\left\lvert\frac{LHS-RHS}{RHS}\right\rvert$	%	2.75	7.83	14.37

In Table 8, it can be seen that the integral thermodynamic consistency test is obeyed fairly well by the binary CO_2-CH_4 adsorption data on silicalite at 40°C, worse at 70°C, and worst at 100°C. Therefore, the binary CO_2-CH_4 adsorption data on silicalite at low temperature satisfy the integral thermodynamic consistency test fairly well. The thermodynamic consistency becomes worse as temperature increases. In addition, the results of the integral thermodynamic consistency test match the results in Fig. 5. At low temperature, the thermodynamic consistency is good while the difference between predictions and experimental data is small in Fig. 5; at higher temperature, the thermodynamic consistency is less satisfied while the difference is big.

CONCLUSIONS

According to the pure gas isotherm data on silicalite, carbon dioxide is adsorbed more than methane. The pure gas adsorption capacity decreases with increasing temperature in the systems of carbon dioxide and methane on silicalite as expected from a physical adsorption system. Among the three concentration pulse chromatographic methods, the HT-CPM is the best one, the MTT-CPM is very well, and the MVV-CPM is not satisfactory for the binary behavior of CO_2/CH_4 on silicalite. The adsorption capacities for CH_4 and CO_2 are very promising for silicalite as an adsorbent in applications in CO_2 removal from landfill gases. q_{CO2}, q_{CH4} and q_{total} increase with decreasing temperature, so temperature is a very important factor for the separation of this system, particularly when y_{CO2} is very low. For predicting the binary system of CO_2/CH_4 with silicalite adsorbent, Flory-Huggins VST, extended Langmuir, extended Dualsite Langmuir, extended Sips, ideal adsorbed solution theory, and the statistical model cannot be used confidently. These models should only be used at low temperatures or for rough estimation when the experimental binary data are not available. The selectivity is very good for the CO_2/CH_4 binary system on silicalite. The CO_2-CH_4 binary adsorption data on silicalite at low temperature satisfy the integral thermodynamic consistency test fairly well. The thermodynamic consistency becomes better as the temperature decreases.

NOMENCLATURE

A	parameter, dimensionless
B	adsorption affinity constant, usually atm^{-1} (units depending on models); parameter, dimensionless
B_0	adsorption affinity constant at some reference temperature, atm^{-1}
B_1	adsorption affinity constant in Site 1, atm^{-1}
B_2	adsorption affinity constant in Site 2, atm^{-1}

C	parameter, dimensionless
K	dimensionless Henry's law constant, dimensionless
K_P	dimensional Henry's law constant, mmole $\cdot$ g^{-1} $\cdot$ atm^{-1}
k	Freundlich adsorption coefficient, mmol $\cdot$ g^{-1} $\cdot$ atm$^{-1/n}$
n	adsorption exponents or number of actives sites, dimensionless
n_0	adsorption exponents at some reference temperature, dimensionless
P	(total) pressure, atm
P_1	pressure of Component 1, atm
P_2	pressure of Component 2, atm
P_A	pressure of Component A, atm
P_B	pressure of Component B, atm
Q	isosteric heat, J $\cdot$ mol^{-1}
q	amount adsorbed, mmol $\cdot$ g^{-1}
q_A	amount adsorbed of Component A, mmol $\cdot$ g^{-1}
q_B	amount adsorbed of Component B, mmol $\cdot$ g^{-1}
q_1	amount adsorbed of Component 1, mmol $\cdot$ g^{-1}
q_2	amount adsorbed of Component 2, mmol $\cdot$ g^{-1}
q_1^0	amount adsorbed of Component 1 in pure system, mmol $\cdot$ g^{-1}
q_2^0	amount adsorbed of Component 2 in pure system, mmol $\cdot$ g^{-1}
q_m	adsorption saturation capacity or maximum amount adsorbed, mmol $\cdot$ g^{-1}
q_{m0}	adsorption saturation capacity or maximum amount adsorbed at some referencetemperature, mmol $\cdot$ g^{-1}
q_{m1}	adsorption saturation capacity or maximum amount adsorbed in Site 1, mmol $\cdot$ g^{-1}
q_{m2}	adsorption saturation capacity or maximum amount adsorbed in Site 2, mmol $\cdot$ g^{-1}
R	gas constant, 8.314 J . K^{-1} $\cdot$ mol^{-1}
T	temperature, K
T_0	reference temperature, K
x	mole fraction in adsorbed phase at equilibrium, dimensionless
x_A	mole fraction of Component A in adsorbed phase at equilibrium, dimensionless
x_B	mole fraction of Component B in adsorbed phase at equilibrium, dimensionless
X_i	mole fraction of Component i in adsorbed phase at equilibrium, dimensionless
y	mole fraction in fluid phase at equilibrium, dimensionless

y_A	mole fraction of Component *A* in fluid phase at equilibrium, dimensionless
y_B	mole fraction of Component B in fluid phase at equilibrium, dimensionless
y_1	mole fraction of Component 1 in fluid phase at equilibrium, dimensionless
Y_i	mole fraction of Component i in fluid phase at equilibrium, dimensionless

Greek Letters

α	adsorption constant, adsorption separation factor, dimensionless
$\alpha_{A/B}$	adsorption separation factor (the ratio of Component A over Component B), dimensionless
$\alpha_{i,A/B}$	ideal adsorption separation factor (the ratio of Component A over Component B), dimensionless
α	parameter, dimensionless
β	parameter, dimensionless
γ_i	activity coefficient of Component i, dimensionless
θ	fraction of monolayer coverage, dimensionless
λ	parameter, dimensionless
Φ_i	fugacity coefficient of Component i, dimensionless
χ	constant parameter, dimensionless

Abbreviations

CPM	Concentration pulse method
DSL	Dualsite-Langmuir
GHG	Greenhouse gases
GSE	Gibbsian surface excess
GWP	Greenhouse warming potential
HT-CPM	Harlick and Tezel-Concentration pulse method
LFG	Landfill gas
MS	Microsoft
MTT-CPM	Modified Triebe and Tezel-concentration pulse method
MVV-CPM	Modified *Van der Vlist and Van der Meijden*-concentration pulse method
PSA	Pressure swing adsorption
RMS	Root mean square
SSR	Sum of the square residuals
TCD	Thermal conductivity detector
TSA	Temperature swing adsorption
VST	Vacancy solution theory

ACKNOWLEDGMENTS

Financial supports received from the Natural Sciences and Engineering Research Council of Canada (NSERC), the Ontario Graduate Scholarship (OGS) Program, and the Canadian Society for Chemical Engineering (CSChE) are gratefully acknowledged.

REFERENCES

1. Cavenati, S., Grande, C.A., and Rodrigues, A.E. (2005) Upgrade of methane from landfill gas by pressure swing adsorption. *Energy and Fuels*, 19: 2545.
2. Hansen, J., Fung, I., Lacis, A., Riud, D., Levedeff, J.S., Ruedy, R., and Russell, G. (1988) Global climate changes as forecast by Goddard institute for space studies three-dimensional model. *Journal of Geophysical Research*, 93: 9341.
3. Cavenati, S., Grande, C.A., and Rodrigues, A.E. (2004) Adsorption equilibrium of methane, carbon dioxide, and nitrogen on zeolite 13X at high pressures. *Journal of Chemical and Engineering Data*, 49: 1095.
4. Buss, E. (1995) Gravimetric measurement of binary gas adsorption equilibria of methane-carbon dioxide mixtures on activated carbon. *Gas Separation and Purification*, 9: 189.
5. Harlick, P.J.E. and Tezel, F.H. (2003) Use of concentration pulse chromatography for determining binary isotherms: comparison with statically determined binary isotherms. *Adsorption*, 9: 275.
6. Harlick, P.J.E. and Tezel, F.H. (2001) CO_2-N_2 and CO_2-CH_4 Binary adsorption isotherms with H-ZSM-5: the importance of experimental data regression with the concentration pulse method. *The Canadian Journal of Chemical Engineering*, 79: 236.
7. Harlick, P.J.E. and Tezel, F.H. (2002) Adsorption of carbon dioxide, methane and nitrogen: pure and binary mixture adsorption by H-ZSM-5 with SiO_2/Al_2O_3 ratio of 30. *Separation Science and Technology*, 37: 33.
8. Harlick, P.J.E. and Tezel, F.H. (2003) Adsorption of carbon dioxide, methane and nitrogen: pure and binary mixture adsorption for ZSM-5 with SiO_2/Al_2O_3 ratio of 280. *Separation and Purification Technology*, 33: 199.
9. Li, P. and Tezel, F.H. (2006) Adsorption separation of methane and carbon dioxide from landfill gas, AICHE (American Institute of Chemical Engineers) Annual Meeting, San Francisco, USA, 64334.
10. Van der Vlist, E. and Van der Meijden, J. (1973) Determination of the adsorption isotherms of the components of binary gas mixtures by gas chromatography. *Journal of Chromatography*, 79: 1.
11. Shah, D.B. and Ruthven, D.M. (1977) Measurement of zeolite diffusivities by chromatography. *AIChE Journal*, 23: 804.
12. Tezel, F.H., Tezel, H.O., and Ruthven, D.M. (1992) Determination of pure and binary isotherms for nitrogen and krypton. *Journal of Colloid and Interface Science*, 149: 197.
13. Heslop, M.J., Buffman, B.A., and Mason, G.A. (1996) Test of the polynomial-fitting method of determining binary-gas-mixture adsorption equilibria. *Industrial and Engineering Chemistry Research*, 35: 1456.

14. Harlick, P.J.E. and Tezel, F.H.A. (2000) Novel solution method for interpreting binary adsorption isotherms from concentration pulse chromatography data. *Adsorption*, 6: 293.
15. Markham, E.C. and Benton, A.F. (1931) The adsorption of gas mixtures by silica. *Journal of American Chemical Society*, 53: 497.
16. Bowen, T.C. and Vane, L.M. (2006) Ethanol, acetic acid, and water adsorption from binary and ternary liquid mixtures on high-silica zeolites. *Langmuir*, 22: 3721.
17. Tien, Chi (1994) *Adsorption Calculations and Modeling*; Butterworth-Heinemann: Newton, MA.
18. Myers, A.L. and Prausnitz, J.M. (1965) Thermodynamics of mixed-gas adsorption. *AICHE J.*, 11: 121.
19. Cochran, T.W., Kabel, R.L., and Danner, R.P. (1985) Vacancy solution theory of adsorption using Flory-Huggins activity coefficient equations. *AICHE J.*, 31: 268.
20. Ruthven, D.M. (1984) *Principles of Adsorption and Adsorption Processes*; John Wiley and Sons: Toronto, Canada.
21. Li, P. and Tezel, F.H. (2007) Adsorption separation of N_2, O_2, CO_2 and CH_4 gases by β-zeolite. *Microporous & Mesoporous Materials*, 98: 94.
22. Li, P. and Tezel, F.H. (2005) Equilibrium and kinetic analysis of CO_2-N_2 adsorption separation by concentration pulse chromatography, 40th IUPAC Congress, Beijing, P. R. China, p. 61, 1–O–034.
23. Triebe, R.W. and Tezel, F.H. (1995) Adsorption of nitrogen and carbon monoxide on clinoptilolite: Determination and prediction of pure and binary isotherms. *The Canadian Journal of Chemical Engineering*, 73: 717.
24. Sircar, S. (1985) Excess properties and thermodynamics of multicomponent gas adsorption. *J. Chem. SOC., Faraday Trans.*, 81: 1527.
25. Rao, M.B. and Sircar, S. (1999) Thermodynamic consistency for binary gas adsorption equilibria. *Langmuir*, 15: 7258.
26. Rees, L.V.C., Bruckner, P., and Hampson, J. (1991) Sorption of N_2, CH_4 and CO_2 in Silicalite-1. *Gas Separation and Purification*, 5: 67.
27. Dunne, J.A., Mariwala, R., Rao, M., Sircar, S.R., Gorte, J., and Myers, A.L. (1996) Calorimetric heats of adsorption and adsorption isotherms. 1. O_2, N_2, Ar, CO_2, CH_4, C_2H_6, and SF_6 on silicalite. *Langmuir*, 12: 5888.
28. Choudhary, V.R. and Mayadevi, S. (1996) Adsorption of methane, ethane, ethylene, and carbon dioxide on Silicalite-1. *Zeolites*, 17: 501.
29. Dubinin, M.M., Rakhmatkariev, G.U., and Isirikyan, A.A. (1989) Heats of adsorption of CO_2 on high-silicon zeolites ZSM-5 and silicalite. *Izv. Akad. Nauk SSSR, Ser. Khim.*, No. 11: 2636.
30. Otto, K., Montreuil, C.N., Todor, O., McCabe, R.W., and Gandhi, H.S. (1991) Adsorption of hydrocarbons and other exhaust hydrocarbons on silicalite. *Ind. Eng. Chem. Res.*, 30: 2333.